



Nanoscale

**UV-Trained and Metal-Enhanced Fluorescence of Biliverdin  
and Biliverdin Nanoparticles**

Journal:	<i>Nanoscale</i>
Manuscript ID	NR-ART-11-2020-008485
Article Type:	Paper
Date Submitted by the Author:	29-Nov-2020
Complete List of Authors:	Fathi, Parinaz; University of Illinois at Urbana-Champaign, Bioengineering Roslend, Ayman; UIUC Mehta, Kritika; UIUC Moitra, Parikshit; University of Illinois at Urbana-Champaign, Bioengineering Zhang, Kai; University of Illinois at Urbana-Champaign, Biochemistry; University of Illinois at Urbana-Champaign, Pan, Dipanjan; UMBC, CHEMICAL, Biochemical and Environmental Engineering; UMB,

SCHOLARONE™  
Manuscripts

## ARTICLE

## UV-Trained and Metal-Enhanced Fluorescence of Biliverdin and Biliverdin Nanoparticles

Parinaz Fathi,<sup>a</sup> Ayman Roslend,<sup>a</sup> Kritika Mehta,<sup>b</sup> Parikshit Moitra,<sup>c</sup> Kai Zhang,<sup>b</sup> and Dipanjan Pan<sup>\*ad</sup>

Received 00th January 20xx,  
Accepted 00th January 20xx

DOI: 10.1039/x0xx00000x

Increasing the fluorescence quantum yield of fluorophores is of great interest for *in vitro* and *in vivo* biomedical imaging applications. At the same time, photobleaching and photodegradation resulting from continuous exposure to light is a major consideration in the translation of fluorophores from research applications to industrial or healthcare applications. A number of tetrapyrrolic compounds, such as heme and its derivatives, are known to provide fluorescence contrast. In this work, we found that biliverdin (BV), a naturally-occurring tetrapyrrolic fluorophore, exhibits an increase in fluorescence quantum yield, without exhibiting photobleaching or degradation, in response to continuous ultraviolet (UV) irradiation. We attribute this increased fluorescence quantum yield to photoisomerization and conformational changes in BV in response to UV irradiation. This enhanced fluorescence can be further altered by chelating BV with metals. UV irradiation of BV led to an approximately 10-fold increase in its 365 nm fluorescence quantum yield, and the most favorable combination of UV irradiation and metal chelation led to an approximately 18.5-fold increase in its 365 nm fluorescence quantum yield. We also evaluated these stimuli-responsive behaviors in biliverdin nanoparticles (BVNPs) at the bulk-state and single-particle level. We determined that UV irradiation led to an approximately 2.4-fold increase in BVNP 365 nm quantum yield, and the combination of UV irradiation and metal chelation led to up to a 6.75-fold increase in BVNP 365 nm quantum yield. Altogether, these findings suggest that UV irradiation and metal chelation can be utilized alone or in combination to tailor the fluorescence behavior of imaging probes such as BV and BVNPs at selected wavelengths.

### Introduction

Organic dyes and nanoparticles can serve as imaging and therapeutic probes for biomedical applications.<sup>1–5</sup> A number of studies have been conducted on nano-structure-related photocontrol and imaging.<sup>6–14</sup> The use of tetrapyrroles as building blocks of self-assembled nanoparticles has been increasingly explored for a variety of applications in diagnosis and treatment of diseases.<sup>15–24</sup> Tetrapyrroles are known for their absorbance, fluorescence, and ability to form complexes with a variety of metals. Naturally-occurring tetrapyrroles include heme, bilirubin and biliverdin (bile pigments resulting from the break-down of heme from hemoglobin), and chlorophyll, among others. Biliverdin is a water-soluble tetrapyrrolic molecule of particular interest due to its near-infrared absorbance,<sup>25</sup> which allows for its use as a photoacoustic contrast agent, in addition to its biodegradation in response to biliverdin reductase, an enzyme available throughout the body and especially in the liver.<sup>26,27</sup> Recently, we reported the synthesis of self-assembled biliverdin nanoparticles (BVNPs) for use in fluorescence

and photoacoustic imaging.<sup>21</sup> BVNPs were found to be enzyme-responsive due to biliverdin's inherent biodegradation pathway, which allowed for the complete degradation of biliverdin nanoparticles *in vitro* and *in vivo*.

The response of tetrapyrroles to external stimuli has long been of interest in utilizing these biologically-active molecules as imaging probes. A number of studies have examined some of the effects of these stimuli on spectral and conformational behavior. Goncharova et al. determined the effect of metal chelation on circular dichroism spectra of biliverdin and bilirubin in chiral matrices.<sup>28</sup> Wagnière et al. examined the effect of conformational structure on the absorbance behavior of biliverdin-human serum albumin complexes.<sup>29</sup> Dimitrijević et al. examined the effect of copper chelation on spectral properties of biliverdin.<sup>30</sup> Ostrow et al. reported that biliverdin undergoes photodegradation *in vitro*, finding that a higher pH led to faster photodecomposition in the presence of fluorescent daylight lamps, with photodecomposition tracked over six hours.<sup>31</sup> The effect of illumination of light on other tetrapyrroles has also been examined,<sup>32,33</sup> and short-term exposure to UV irradiation has been shown to lead to enhancement of hemoglobin fluorescence emission<sup>34</sup>. Interestingly, Rotomskis et al. proposed that hematoporphyrin undergoes two competing processes in response to illumination: photodegradation and the formation of stable photoproducts.<sup>33</sup>

Despite this, the individual and combined effects of metal chelation and UV irradiation on biliverdin's spectral properties and conformational structure, as well as their ability to increase fluorescence quantum yield, has not been explored. Additionally, the ability of these altered spectral properties to be transferred to tetrapyrrole-based nanoparticles has also not been reported. With

<sup>a</sup> Departments of Bioengineering, Materials Science and Engineering, and Beckman Institute, University of Illinois at Urbana-Champaign, Urbana, Illinois 61801, U.S.

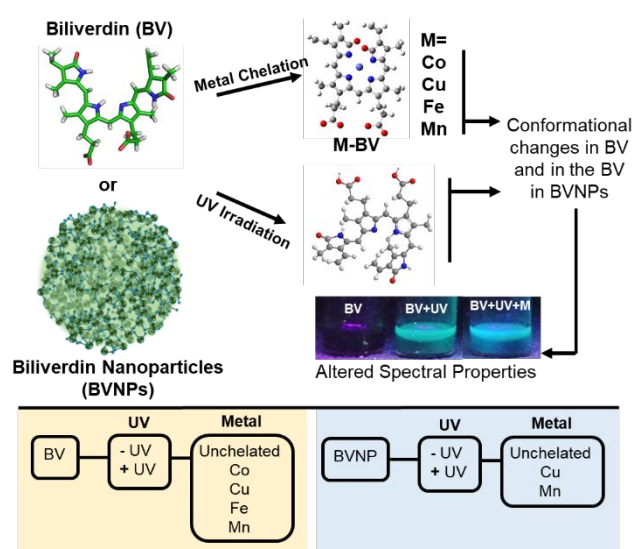
<sup>b</sup> Department of Biochemistry, School of Molecular and Cellular Biology, University of Illinois at Urbana-Champaign, Urbana, Illinois 61801, U.S.

<sup>c</sup> Department of Pediatrics, University of Maryland School of Medicine, Baltimore, MD 21201, U.S.

<sup>d</sup> Departments of Diagnostic Radiology Nuclear Medicine, Pediatrics, and Chemical and Biomolecular Engineering, University of Maryland School of Medicine and University of Maryland Baltimore County, Baltimore, MD 21201, U.S.

\*dipanjan@som.umaryland.edu

the increasing use of tetrapyrrolic nanoparticles for biomedical applications, a better understanding of their response to stimuli would provide a clear path to manipulating the spectroscopic properties of these particles for applications in bioimaging. Although biliverdin does not fluoresce in the near-infrared region, its fluorescence in the UV-visible range can be used for *in vitro* imaging applications. The goal of this work was to determine the effects of UV irradiation and metal chelation on biliverdin's spectral properties, and whether these effects could be exploited for use in enhancing the spectral properties of biliverdin nanoparticles (**Scheme 1**). The effects of UV irradiation were of particular interest because in contrast to what we expected based on previous reports, we found that not only did UV irradiation not lead to photodegradation of biliverdin, it additionally led to enhancement of biliverdin's fluorescence emission for select wavelengths. We also examined the effects of metal chelation and UV irradiation on BVNP behavior at the single-particle level, including studying the photoblinking and photobleaching behavior of these particles. To the best of our knowledge, this is also the first report of the photophysical behavior of tetrapyrrole-derived nanoparticles at the single-particle level.



**Scheme 1.** Biliverdin (BV) undergoes conformational changes as a result of metal chelation or 72 h of 365 nm UV irradiation. These conformational changes lead to enhanced fluorescence emission. Similarly, the biliverdin in biliverdin nanoparticles (BVNPs) can also undergo conformational changes in response to these stimuli, leading to alterations in BVNP spectral properties.

## Results and Discussion

In order to establish the separate and combined effects of metal chelation and UV irradiation on the spectral properties of molecular biliverdin (BV) and self-assembled biliverdin nanoparticles (BVNPs), we conducted a series of experiments in which molecular biliverdin and biliverdin nanoparticles were exposed to metal chloride solutions and subsequently illuminated with 365 nm UV irradiation for 72 hours. The irradiation wavelength was selected because of biliverdin's fluorescence emission for 365 nm excitation, while the irradiation time was established through experimentation. Further experiments with other irradiation wavelengths and times should be conducted in the future to further explore the wider applicability of the system for various biomedical applications. Detailed methods are provided in the Supplementary Information. BV and BVNPs were

then spectroscopically characterized to determine the roles of metal chelation and UV irradiation in inducing conformational changes that led to altered spectral properties. BVNPs were further imaged using single-particle imaging to allow for comparison of bulk-state and single-particle properties of these nanoparticles.

**Formation of metal-BV chelates and evaluation of UV stability.** BV was exposed to cobalt (II) chloride, copper (II) chloride, iron (III) chloride, or manganese (II) chloride and subsequently irradiated with UV light for 72 h. To confirm the formation of metal-BV complexes, and determine the stability of BV in the presence of UV irradiation, we collected FT-IR spectra (**Fig. 1A**). For BV alone, we identified N-H bending ( $\approx 3300\text{ cm}^{-1}$ ), C=O stretching ( $\approx 1700\text{ cm}^{-1}$ ), C=C stretching ( $\approx 1600\text{ cm}^{-1}$ ), O-H bending from carboxylic acid ( $\approx 1400\text{ cm}^{-1}$ ), and C-O stretching ( $\approx 1100\text{ cm}^{-1}$ ) peaks. The FT-IR spectra exhibited no change as a result of UV irradiation, demonstrating the stability of biliverdin even after long-term UV irradiation. Upon metal chelation, the characteristic FT-IR peak between  $1050\text{ cm}^{-1}$  and  $1200\text{ cm}^{-1}$  exhibited a sharpening which correlated with the peaks observed for the metal salt solutions. Since complexation between biliverdin and transition metal ions occurs through the formation of M-N bonds in place of two H-N bonds within the tetrapyrrole structure, we observed changes in the N-H bending peak ( $\approx 3300\text{ cm}^{-1}$ ) after metal chelation. The proposed metal chelate structures are provided in **Fig. 1B**, with the assumption that each biliverdin molecule chelates a single metal ion. To obtain further confirmation that UV irradiation did not lead to degradation of biliverdin, we conducted mass spectrometry on BV samples before and after UV irradiation (**Fig. 1C**). In both cases, the peak characteristic of BV+H<sup>+</sup> at an m/z value of approximately 583 is observed. There are no new peaks that appear after 72 h of UV irradiation, which confirms that BV has not degraded as a result of the treatment.

**Effects of metal chelation and UV irradiation on BV absorbance and fluorescence.** The effects of metal chelation alone, UV irradiation alone, and the combined effects of metal chelation and subsequent UV irradiation on the spectroscopic properties of BV were apparent upon visual examination. Under white light, the color of BV samples that were chelated with metals changed based on the metal used (**Fig. 2A**). There were no visible differences in sample color under white light for samples treated with 72 h of UV irradiation and those not treated with UV irradiation. When BV and metal-chelated BV samples were UV irradiated for 72 h, they exhibited a bright fluorescence when illuminated with 365 nm light (**Fig. 2A**). The fluorescence emission of unchelated BV appeared green, while the fluorescence emission of cobalt-chelated BV (Co-BV), copper-chelated BV (Cu-BV), iron-chelated BV (Fe-BV), and manganese-chelated BV (Mn-BV) appeared blue.

The absorbance spectra of porphyrin and tetrapyrrolic molecules are typically composed of a Soret band (400–436 nm), Q bands (490–650 nm), and N, L, and M bands (200–350 nm).<sup>35,36</sup> The Soret band, which is attributed to the strong transition from  $S_0$  to the second excited state  $S_2$ , has a greater intensity than Q bands. The weak transition from  $S_0$  to the first excited state  $S_1$  is associated with the Q bands.<sup>35,36</sup> Chelation of BV with all tested metals generally decreased UV-visible light absorption between 230 nm and 450 nm, as well as between 550 nm and 800 nm (**Fig. 2B**), thus affecting both the  $S_0$  to  $S_1$  and  $S_0$  to  $S_2$  transitions. Mn-BV and Co-BV in particular exhibited not only a dramatic decrease in absorption, but also caused the appearance of new absorption peaks between 230 nm and 450 nm, as well as between 550 nm and 800 nm. In contrast, UV

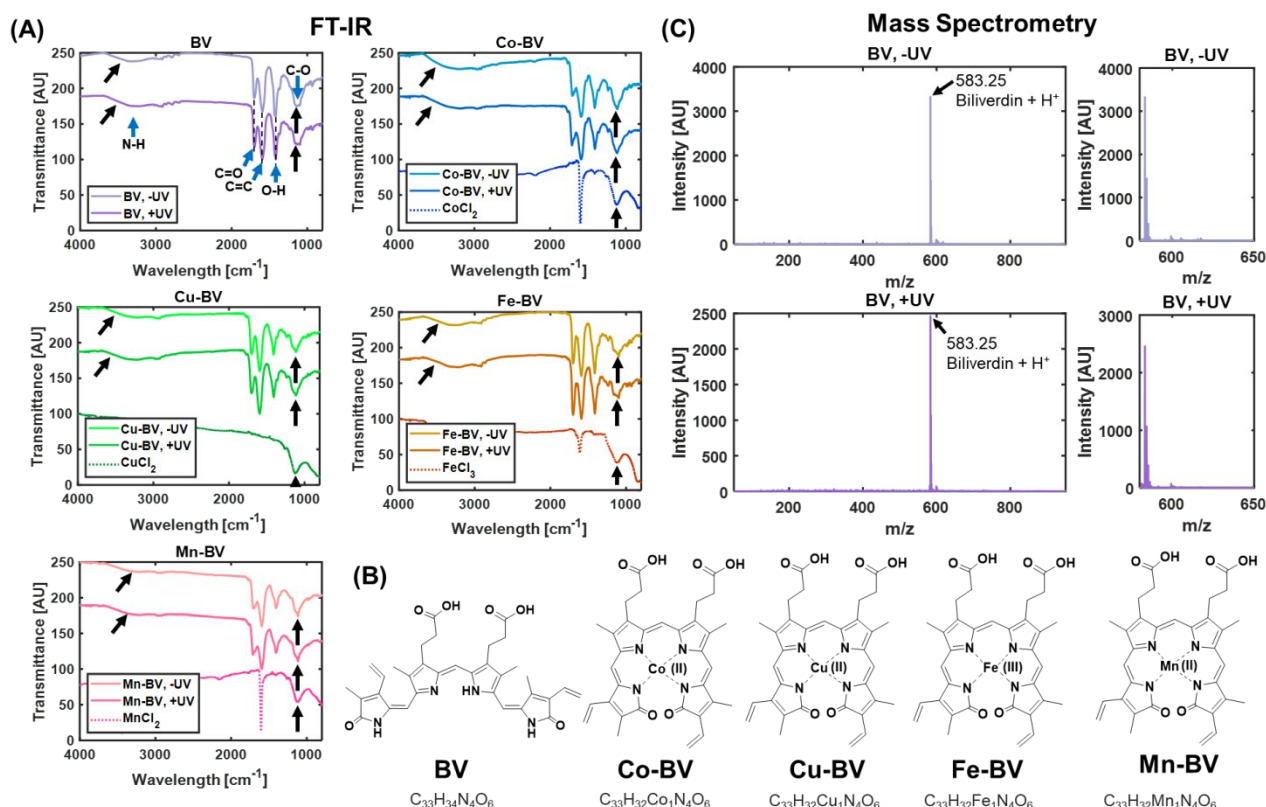


**Figure 1.** Formation and stability of BV metal chelates. (A) FT-IR spectra of BV and BV metal chelates. Black arrows identify peaks that are altered as a result of metal chelation. The chelation and presence of metals in the BV metal chelates are confirmed by changes in shape of peaks between 3000 cm<sup>-1</sup> and 4000 cm<sup>-1</sup>, and peaks between 1050 cm<sup>-1</sup> and 1200 cm<sup>-1</sup>. There is no apparent change as a result of UV irradiation. (B) Structures of BV and its metal chelates. Dashed lines represent chelation/coordinate bond formation. Each chelated metal displaces two hydrogen atoms in the BV structure. (C) Mass spectra of BV without UV irradiation and after 72 h of UV irradiation. The presence of BV characteristic peak and lack of appearance of new peaks of smaller masses indicates BV is not degrading as a result of the UV irradiation. Altogether these results confirm BV metal chelate formation and BV stability in the face of exposure to long-term UV irradiation.

irradiation of both BV and metal-chelated BV samples did not significantly alter UV-visible light absorption (Fig. 2B). Ratios of final (after UV irradiation) to initial (without UV irradiation) 365 nm absorbance and 680 nm absorbance confirm that finding (Fig. S1). Importantly, the effects of metals on the absorbance ratios remained similar, regardless of whether or not the samples were exposed to UV irradiation. This suggests that any conformational changes resulting from UV irradiation do not remove the chelated metals from BV. Fe-BV absorbance was the most similar to BV absorbance, while Cu-BV, Mn-BV, and Co-BV had decreased absorbances.

72 h of UV irradiation dramatically increased the fluorescence of both BV and metal-chelated BV samples (Fig. 2C, Fig. 2D (i)). However, the fluorescence intensities did not scale with the 365 nm absorbance, which suggests that metal chelation and UV irradiation each alter the quantum yield of biliverdin. Importantly, although the absorbance spectra of metal-chelated BV had some differences from that of BV alone, we compared the fluorescence intensities of all samples using the same excitation wavelengths since quantum yield of a molecule can differ from one excitation wavelength to another. We observed the largest increase in fluorescence intensity for BV (14-fold) and Cu-BV (10-fold) (Fig. 2D (ii)). The changes in Fe-BV and Mn-BV fluorescence intensities (approximately 5-fold each) were lower than that of unchelated BV. Without 72 h of UV irradiation, metal-chelated BV samples exhibited a 1.3 to 2-fold greater fluorescence than unchelated BV when excited at 365 nm (Fig. 2D (iii)). Notably, metal-chelated samples that were also UV-irradiated showed fluorescence intensities comparable to, or less than, the

fluorescence intensity of UV-irradiated unchelated BV (Fig. 2D (iv)). In addition, 72 h UV irradiation also caused a slight blue-shifted fluorescence emission in all samples (Fig. S2).

Our results suggest that biliverdin's 365 nm fluorescence emission can be separately enhanced by either metal chelation or UV irradiation. While metal chelation causes a small increase in fluorescence (1.3 to 3-fold), UV irradiation has a much greater effect (2 to 14-fold). However, metal chelation attenuates the effects of UV irradiation on BV fluorescence intensity. Additionally, since quantum yield is a ratio of the photons emitted to photons absorbed, the increase in fluorescence intensity for 365 nm excitation, coupled with decreased 365 nm absorbance, for metal-chelated BV, indicates that metal chelation resulted in an increase in quantum yield at this excitation wavelength.

For an excitation wavelength of 488 nm, the fluorescence trends differ from those at an excitation wavelength of 365 nm (Fig. S3). With 488 nm excitation, 72 h of 365 nm UV irradiation results in a decrease in BV fluorescence intensity, with no apparent effect on the fluorescence intensity of BV metal chelates. Chelation with Mn and Co led to an enhancement of fluorescence, while chelation with Cu and Fe led to a quenching of fluorescence. Furthermore, the fluorescence emission peak for 488 nm excitation appears unaffected by the application or absence of 72 h of UV irradiation (Fig. S4). These results suggest that the excitation wavelength utilized for the 72 h UV irradiation may play a role in what excitation wavelengths can be utilized when taking advantage of the UV-induced fluorescence enhancement. Thus, it is possible to "train" BV

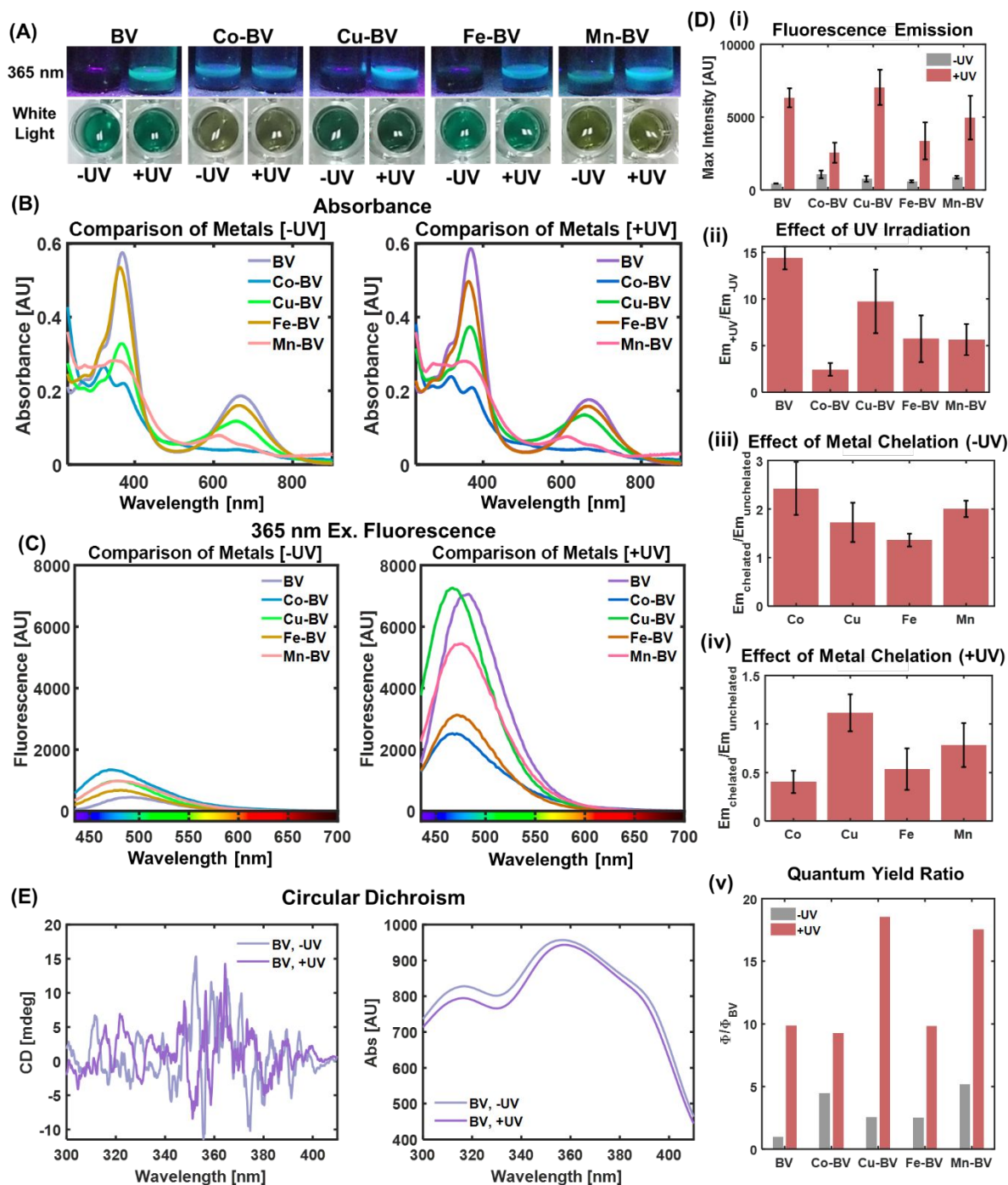


**Figure 2.** Absorbance and fluorescence behavior of BV. **(A)** Visual appearance of samples with and without metal chelation, and with and without 72 h UV irradiation. Samples are illuminated with ambient white light (bottom) and 365 nm light (top). Under illumination by white light, it is apparent that metal chelation leads to changes in sample color. Under UV irradiation, it is apparent that metal chelation leads to blue-shifted fluorescence emission. Furthermore, 72 h UV irradiation causes an increase in fluorescence intensity under 365 nm UV illumination. Ambient light images are of samples diluted to 25% of their final concentration in order to better show their colors. **(B)** UV-visible absorption spectra of BV samples without UV irradiation and after 72 h of UV irradiation. Metal chelation leads to decreased absorbance. **(C)** Fluorescence spectra of BV samples without UV irradiation and after 72 h of UV irradiation. UV irradiation enhances fluorescence intensity. An excitation wavelength of 365 nm and gain of 100 was used. **(D)** Effects of metal chelation and UV irradiation on the fluorescence emission of BV for 365 nm excitation. Error bars represent standard deviation obtained with three separate experiments. **(i)** Average fluorescence intensity for BV and metal chelates with and without 72 h UV irradiation. UV irradiation and metal chelation each enhance fluorescence emission. **(ii)** Average ratio of fluorescence intensity with UV irradiation to fluorescence intensity without UV irradiation. UV irradiation alone leads to an approximate 3-fold to 14-fold increase in fluorescence intensity. **(iii)** Average ratio of fluorescence intensity with metal chelation to fluorescence intensity without metal chelation, in the absence of UV irradiation. Metal chelation alone leads to slight increases in fluorescence intensity. **(iv)** Average ratio of fluorescence intensity with metal chelation to fluorescence intensity without metal chelation, after 72 h UV irradiation. In cases where both UV irradiation and metal chelation were used, chelation led to either no change in fluorescence intensity, or a decrease in fluorescence intensity compared to UV-irradiated unchelated samples. **(v)** Fluorescence quantum yield expressed as a ratio to that of BV. Metal chelation and UV irradiation each increase the quantum yield compared to that of BV. **(E)** Circular dichroism spectra of BV and UV-irradiated BV. UV irradiation leads to flipping of circular dichroism peaks. This indicates the occurrence of conformational changes as a result of UV irradiation.

for an enhanced response to 365 nm excitation, by long-term exposure of BV to that wavelength.

#### Effects of stimuli and excitation wavelength on BV quantum yield.

The effects of metal chelation and UV irradiation on BV fluorescence and absorbance behavior suggested that these stimuli led to changes in fluorescence quantum yield. To assess this, we calculated the relative quantum yield of BV and its metal chelates for 365 nm and 488 nm excitation using reference dyes Quinine Sulfate and Rhodamine 6G, respectively (Table 1, Fig. 2D(v), Fig. S5). For 365 nm excitation, the quantum yield of BV alone is quite low (0.012 %), but UV irradiation leads to an almost 10-fold increase in quantum yield (0.119 % at 365 nm). Metal chelation and UV irradiation each led to an increase in 365 nm quantum yield, although the gains from metal chelation alone were modest compared to those of UV irradiation or combined metal chelation and UV irradiation. For example, copper chelation leads to an approximately 2.6-fold enhancement in BV quantum yield, while combined copper chelation and UV irradiation lead to an approximately 18.5-fold enhancement.

Furthermore, we found that the quantum yield of biliverdin and its metal chelates were generally higher for an excitation wavelength of 488 nm than 365 nm. This is a reflection of both a higher fluorescence intensity for 488 nm excitation, and a lower 488 nm absorbance, as both of these parameters are taken into consideration for calculation of quantum yield. For 488 nm excitation, BV has a quantum yield of 0.095 %, an almost 8-fold improvement over its quantum yield at 365 nm. 72 h of 365-nm UV irradiation leads to an overall increase in the 488 nm quantum yield of BV.

**Table 1. Relative Fluorescence Quantum yields of BV and its metal chelates**

	365 nm QY [%]		488 nm QY [%]	
	-UV	+UV	-UV	+UV
BV	0.012	0.119	0.095	0.134
Co-BV	0.053	0.111	0.151	0.177
Cu-BV	0.031	0.222	0.080	0.049
Fe-BV	0.030	0.118	0.123	0.078
Mn-BV	0.062	0.210	0.102	0.129

#### Potential Mechanisms Behind Enhanced Quantum Yield of BV.

The effects of UV irradiation and metal chelation on BV quantum yield, coupled with the elimination of possible photodegradation processes by FT-IR and mass spectrometry, suggest that the observed changes may be a result of conformational changes and isomerization. Indeed, the photoisomerization of the C15=C16 double bond between the C- and D-rings in biliverdin and other tetrapyrroles, which leads to rotation of the D-ring, have been previously reported.<sup>37–40</sup> Although these studies have primarily focused on red-light excitation, the photoisomerization of biliverdin by UV irradiation can potentially provide an explanation for our observations. In biliverdin-containing phytochromes, the photoisomerization of biliverdin is followed by further conformational rearrangements of biliverdin and the protein.<sup>37,39,41</sup> We collected circular dichroism (CD) spectra for BV and BV metal chelates with and without 72 h of 365 nm UV irradiation (Fig. 2E, Fig. S6). Since circular dichroism depends on differential absorption of circularly-polarized light, it is widely used to determine the conformation of molecules, with changes in CD spectra corresponding to changes in conformation. It is apparent that UV

irradiation leads to a conformational change in BV, specifically leading to the flipping of circular dichroism peaks at approximately 315 nm, 330 nm, 350 nm, 360 nm, and 375 nm. Additionally, chelation of metals even without UV irradiation led to some peak shifting and flipping with respect to those of BV. Most notably, one or more of the peaks at approximately 350 nm, 360 nm, and 375 nm are flipped in Cu-BV, Fe-BV, and Mn-BV. Flipping of CD peaks and changes in CD peak intensity as a result of metal chelation have previously been reported for biliverdin-metal complexes.<sup>28</sup> Additionally, the magnitude of peaks in Co-BV and Mn-BV are much lower than those of BV alone, indicating that metal chelation leads to different changes in biliverdin's differential absorption of polarized light based on the specific metal that has been chelated. Thus, cobalt and manganese, which led to more drastic changes in absorbance spectra than iron and copper, also led to a more dramatic change in CD spectra than iron and copper. These spectra are different in shape from previously reported spectra because they were collected without complexation of biliverdin within a matrix, in contrast to some previous reports.<sup>28</sup> These data altogether suggest a change in biliverdin's conformation as a result of the applied stimuli. This is a highly reasonable observation considering that open-chain tetrapyrroles can theoretically adopt 64 different isomers, and the fluorescence of biliverdin-derived molecules has been shown to depend on their conformational change.<sup>42</sup>

#### Density Functional Theory (DFT) studies of metal-chelated BV structures.

The conformational flexibility of tetrapyrroles plays an important role in their biological functions.<sup>43</sup> To further explore the effect of metal chelation on BV conformation and the resulting spectral properties, we performed density functional theoretical calculations. It can be said from the energy minimized geometries of the metal complexes that the metal coordination restricted the flexibility of the tetrapyrrole rings of BV (Fig. 3A). This supports our observation that metal chelation attenuates the effects of UV irradiation on BV fluorescence intensity, which is likely a result of the restricted flexibility of metal-chelated BV. The electronic energy diagram and molecular orbital of the geometry optimized structures were then analyzed. It can be seen that HOMO is largely located on the carboxylic acid group whereas LUMO is largely located on the tetrapyrrole rings for BV. The energy gap ( $\Delta E$ ) between  $E_{\text{HOMO}}$  and  $E_{\text{LUMO}}$ , which is an important parameter to determine the charge transfer interaction and chemical stability of a molecule, was also calculated (Fig. 3B). The order of increasing  $\Delta E$  from 1.31 eV (949.4 nm) for Mn-BV, 1.35 eV (918.7 nm) for Co-BV, 1.39 eV (895.3 nm) for Cu-BV, 1.43 eV (868 nm) for Fe-BV to 1.44 eV (863 nm) for BV closely corroborates with the NIR absorbance starting wavelength for the compounds (Fig. 3B and Fig. S7), with a higher starting wavelength apparent for Mn-BV and Co-BV compared to BV, Cu-BV, and Fe-BV. This indicates good overlap between DFT calculations and experimentally collected spectra. Furthermore, although the generation of higher energy gap sites have been shown to lead to enhanced fluorescence (for example, in conjugated polymer backbones<sup>44,45</sup>), metal chelation by biliverdin led to a decrease in the energy gap. Thus, the enhancement of BV fluorescence by metal chelation is likely not a result of changes in the HOMO-LUMO energy gap but rather due to changes in the molecular conformation.

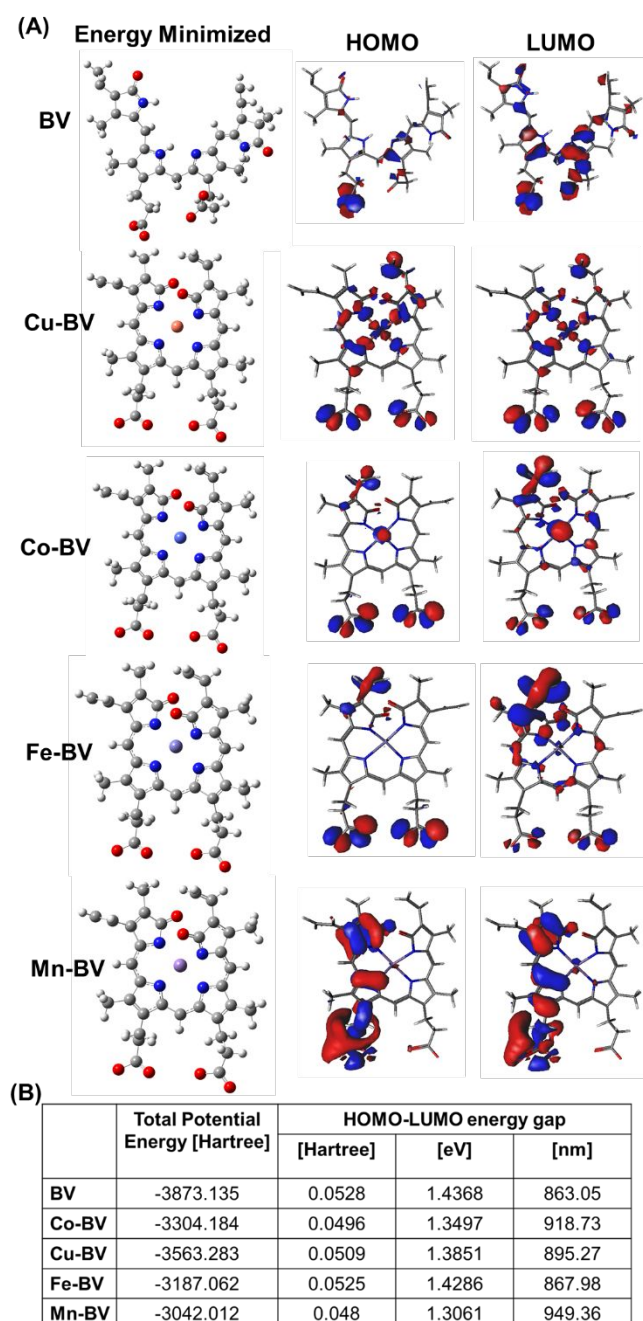


**Figure 3.** Density Functional Theory (DFT) results. (A) Energy minimized structures together with the HOMO-LUMO surface maps are shown for BV, Cu-BV, Co-BV, Mn-BV, and Mn-BV. Metal chelation leads to changes in the HOMO-LUMO surface maps of biliverdin, with Mn-BV showing more drastic changes overall than Cu-BV. Since HOMO-LUMO surface maps illustrate electron density, it is apparent that chelation of different metals has different effects on electron density within the molecules. (B) Corresponding total potential energy and HOMO-LUMO energy gaps for BV, Co-BV, Cu-BV, Fe-BV, and Mn-BV. Metal chelation leads to an increase in the HOMO-LUMO energy gap.

**Effects of metal concentration on BV absorbance and fluorescence (Stern-Volmer analysis).** The Stern-Volmer method was employed to evaluate the effects of metal concentration on BV absorbance and fluorescence behavior. Metal chelation experiments were conducted with higher (100 X, 10 X) and lower (0.1 X and 0.01 X) metal concentrations than reported above. As metal concentration was increased, the absorbance behavior of metal-BV chelates was more dramatically altered (Fig. S8). In general, an increase in metal concentration led to a decrease in 365 nm absorbance (Fig. S9) and 670 nm absorbance (Fig. S10). Furthermore, the fluorescence emission enhancement for 365 nm excitation also depended on the metal concentration. Stern-Volmer plots of fluorescence intensity as a function of metal concentration were obtained (Fig. S11, Fig. S12). For 365 nm excitation, we observed that low metal concentrations led to lower fluorescence emission intensities than samples chelated with 1 X and 10 X concentrations of metal (Fig. S11). For 488 nm excitation, higher metal concentrations generally led to lower fluorescence emission intensities (Fig. S12). This indicates that there is generally a positive correlation between metal concentration and fluorescence emission for 365 nm excitation, and generally a negative correlation between metal concentration and fluorescence emission for 488 nm excitation. Thus, in using metal chelation as a means of biliverdin fluorescence enhancement, one must take into consideration that the same concentration of a metal can result in different effects on fluorescence response to 365 nm excitation and fluorescence response to 488 nm. At the same time, metal chelation, even with only small amounts of metal, is an effective way of altering biliverdin's fluorescence behavior.

**Synthesis of BVNPs and evaluation of UV stability.** The formation and stability of BVNPs was confirmed with mass spectrometry of BVNPs before and after UV irradiation (Figure S13A). In both cases, the characteristic peak at an  $m/z$  value of approximately 583 is observed, in addition to peaks at higher masses, corresponding to the formation of BVNPs from biliverdin. There are no new peaks that appear after 72 h of UV irradiation, which confirms that BVNPs are not being degraded by UV light. This was also confirmed by FT-IR spectroscopy (Fig. S13B), which depicts no changes in the spectra of UV-irradiated BVNPs compared to non-irradiated BVNPs.

**Formation of metal-BVNP chelates and evaluation of their UV stability.** BVNPs were exposed to either copper (II) chloride, or manganese (II) chloride. Copper and manganese were chosen for these experiments for two reasons. First, because Cu-BV and Mn-BV had the highest and lowest total potential energy magnitudes respectively, of all the metal-chelated BV combinations. Second, when combined with UV irradiation in the molecular BV experiments, Cu-BV and Mn-BV had the highest 365-nm fluorescence intensities of all tested metals.

FT-IR spectroscopy was utilized to confirm that metals were successfully chelated within the BVNPs (Fig. S13B). As with metal-BV chelates, metal chelation by the BVNPs led to a sharpening of the peak between  $1050\text{ cm}^{-1}$  and  $1200\text{ cm}^{-1}$ , which is correlated with the peaks observed for the metal salt solutions. The FT-IR spectra of metal-BV chelates exhibited little or no change as a result of UV irradiation.

The color of BVNP samples under white light changed based on the chelated metal (Fig. 4A). Similar to their molecular BV chelate counterparts, Cu-BVNPs and Mn-BVNPs had blue-green and olive-green hues respectively. As we observed with BV, there were no visible differences in BVNP sample color under white light for

samples treated with UV irradiation and those not treated with UV irradiation. Transmission electron microscopy (TEM) images of BVNPs and metal-chelated BVNPs before and after 72 h UV irradiation show no apparent changes in BVNP appearance (Fig. 4B). This further confirms that the particles are stable even under long-term UV exposure.

**Effects of metal chelation and UV irradiation on BVNP absorbance and fluorescence.** UV-visible spectra (Fig. 4C) for chelated and

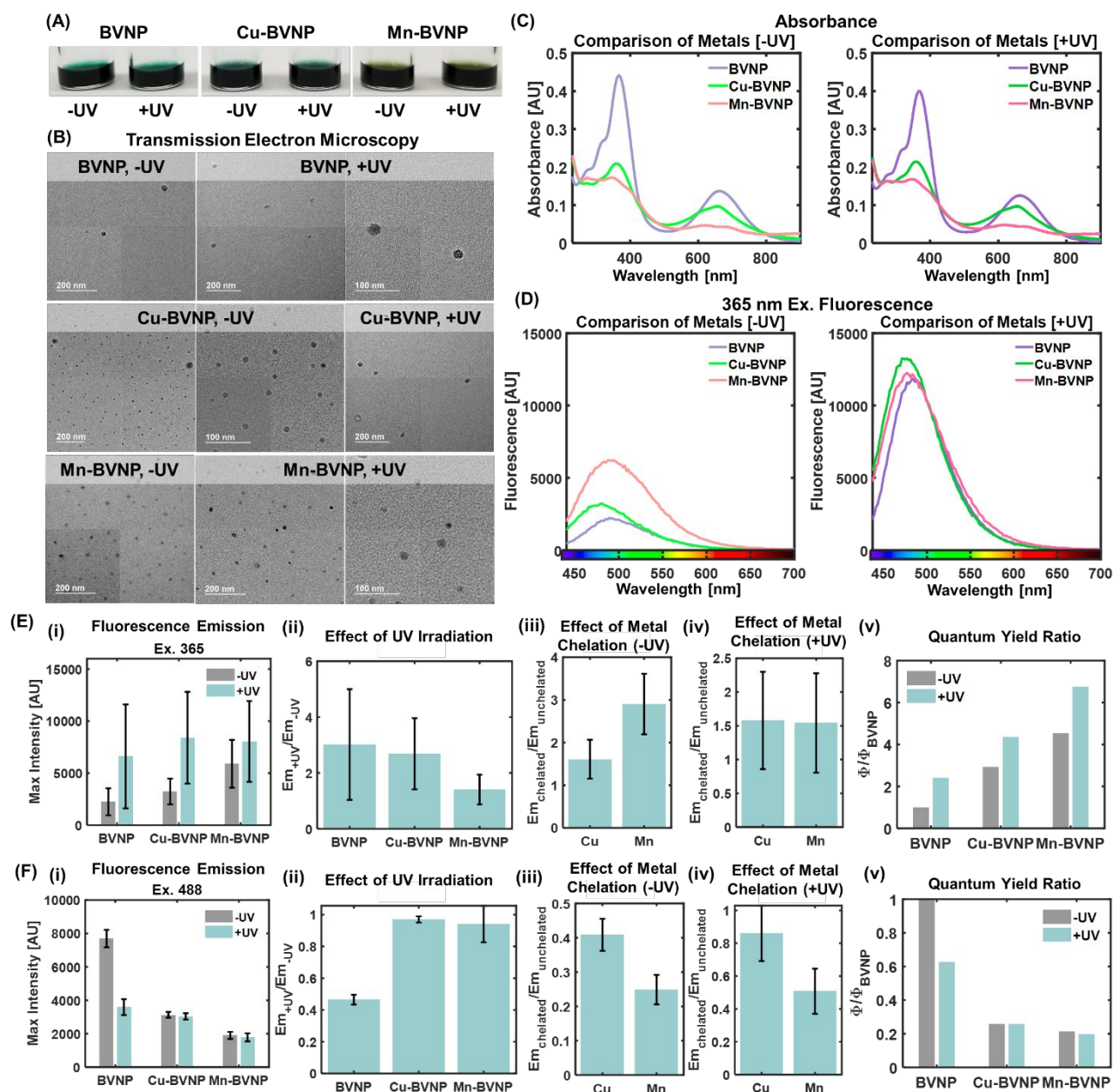


**Figure 4.** Absorbance and fluorescence behavior of BVNPs. (A) Appearance of samples with and without 72 h UV exposure, as well as with and without metal chelation. Samples are illuminated with ambient white light. The solution color differs based on the metal chelated. (B) Transmission electron microscopy images of BVNPs and metal-chelated BVNPs before and after 72 h of 365 nm UV irradiation. Presence of particles after UV irradiation indicates that particles have not degraded as a result of UV exposure. (C) UV-visible absorption spectra of BVNP samples without UV irradiation and after 72 h of UV irradiation. Metal chelation leads to attenuated absorbance similar to the effects of metal chelation on BV. (D) Fluorescence spectra of BVNP samples without UV irradiation and after 72 h of UV irradiation. UV irradiation enhances fluorescence intensity. An excitation wavelength of 365 nm and gain of 150 was used. (E) Average fluorescence intensity for 365 nm excitation. Error bars represent standard deviation across three trials. (i) Average fluorescence intensity for BVNPs with and without 72 h UV irradiation. Metal chelation and UV irradiation each appear to lead to some increases in fluorescence intensity, although error bars overlap. (ii) Average ratio of fluorescence intensity with UV irradiation to fluorescence intensity without UV irradiation. UV irradiation alone leads to some increases in fluorescence intensity. (iii) Average ratio of fluorescence intensity with metal chelation to fluorescence intensity without metal chelation, in the absence of UV irradiation. Metal chelation alone leads to some increases in fluorescence intensity. (iv) Average ratio of fluorescence intensity with metal chelation to fluorescence intensity without metal chelation, after 72 h UV irradiation. Combination of UV irradiation and metal chelation leads to a slight increase in fluorescence intensity that does not appear to depend on the specific metal chelated. (v) 365 nm fluorescence quantum yield expressed as a ratio to that of BVNP. Metal chelation and UV irradiation each increase the quantum yield compared to that of BVNP. (F) Average fluorescence intensity for 488 nm excitation. Error bars represent standard deviation across three trials. (i) Average fluorescence intensity for BVNPs with and without 72 h UV irradiation. (ii) Average ratio of fluorescence intensity with UV irradiation to fluorescence intensity without UV irradiation. (iii) Average ratio of fluorescence intensity with metal chelation to fluorescence intensity without metal chelation, in the absence of UV irradiation. (iv) Average ratio of fluorescence intensity with metal chelation to fluorescence intensity without metal chelation, after 72 h UV irradiation. (v) 488 nm fluorescence quantum yield expressed as a ratio to that of BVNP. Metal chelation and UV irradiation each decrease the quantum yield compared to that of BVNP.

unchelated BVNP samples exhibited a decrease in absorption as a result of chelation. The spectra shapes for Cu-BVNPs and Mn-BVNPs are consistent with the shapes of the spectra for Cu-BV and Mn-BV respectively. The BVNP Q band appears blue-shifted in Cu-BVNPs, and multiple Q band peaks are observed for Mn-BVNPs. UV irradiation did not appear to have as great of an impact on the absorption spectra. Ratios of final (after UV irradiation) to initial (without UV irradiation) 365 nm absorbance and 680 nm absorbance of BVNPs exhibited little to no change in absorbance as a result of UV irradiation (Fig. S14). As in BV samples, the effects of metal chelation on BVNP absorbance ratios remained similar, regardless of whether or not the samples were exposed to UV irradiation.

Representative BVNP fluorescence spectra for 365 nm excitation illustrate an increase in fluorescence after 72 h of UV irradiation (Fig. 4D). There did not appear to be a shift in fluorescence emission as a result of metal chelation or UV irradiation (Fig. S15). For 365 nm excitation, UV irradiation appeared to lead to an increase in fluorescence intensity (Fig. 4E (i)), although the standard deviations for average fluorescence intensity of the UV-irradiated samples overlapped with those of the non-irradiated samples. The ratio of fluorescence intensity with irradiation to fluorescence intensity without irradiation was also lower in BVNP samples compared to BV samples, with a less than 4-fold increase in fluorescence after 72 h of irradiation. This can be explained by restrictions in conformational changes of BV molecules that have been crosslinked into BVNPs. The self-assembly of cross-linked BVNPs likely leads to steric hindrance, which can limit the extent of deformation that individual biliverdin molecules within the BVNPs can undergo. This in turn would be reflected in the spectral properties of the particles. In addition, the lower initial fluorescence intensity of BVNPs compared to BV, even when utilizing a higher gain for BVNP spectra, reveals that BV molecules undergo fluorescence quenching when assembled into BVNPs. Without UV irradiation, chelation of Mn into BVNPs (Mn-BVNPs) led to an approximately 3-fold increase in fluorescence intensity, while chelation of Cu into BVNPs (Cu-BVNPs) led to an approximately 1.5-fold increase in fluorescence intensity (Fig. 4E (iii)). With UV irradiation, the effects of Cu chelation and Mn chelation are indistinguishable from each other, each having only a 1.5-fold increase in fluorescence intensity compared to BVNPs (Fig. 4E (iv)). Thus, it appears that in molecular BV, the effects of UV irradiation on fluorescence behavior are much more pronounced than those from metal chelation, while in BVNPs the individual contributions from UV irradiation and metal chelation are approximately equal. This is likely due to limited deformation of BV molecules within the crosslinked BVNP structure.

For 488 nm excitation, the fluorescence intensity was highest for BVNPs without UV irradiation or metal chelation (Fig. 4F (i)). UV irradiation led to a decrease in BVNP fluorescence intensity, but had no effect on the fluorescence intensities of Cu-BVNP and Mn-BVNP (Fig. 4F (ii)). Without UV irradiation, Cu-BVNP fluorescence was higher than that of Mn-BVNP fluorescence, although both had a lower fluorescence than that of BVNP alone (Fig. 4F (iii)). With UV irradiation, Cu-BVNP fluorescence was again higher than that of Mn-BVNP, although they were both closer to that of BVNP (Fig. 4F (iv)).

**Effects of stimuli and excitation wavelength on BVNP quantum yield.** As with BV, the changes in spectroscopic behavior of BVNPs as a result of metal chelation and UV irradiation suggested a change in its quantum yield. For 365 nm excitation, the relative quantum yields of BVNP and its metal chelates (Table 2) were lower than that of BV itself. This indicates potential fluorescence quenching effects as a

result of BVNP formation. As with BV, exposure of BVNPs to UV irradiation or metal chelation led to an increase in 365 nm fluorescence quantum yield (Fig. 4E (v)). Manganese chelation with UV irradiation led to a combined 6.75-fold increase in 365 nm quantum yield compared to BVNP.

On the other hand, the 488 nm quantum yield of BVNPs was higher than that of BV. This indicates that the BVNP fluorescence self-quenching behavior observed for 365 nm excitation is not at play for 488 nm excitation. Additionally, the higher quantum yield of BVNPs at 488 nm compared to BVNPs at 365 nm is in line with observations for BV quantum yield. For 488 nm excitation, UV irradiation and metal chelation were each determined to lead to a reduction in quantum yield (Fig. 4F (v)).

**Table 2. Relative Fluorescence Quantum Yield of BVNP and its metal chelates.**

	365 nm QY [%]		488 nm QY [%]	
	-UV	+UV	-UV	+UV
BVNP	0.004	0.011	0.448	0.281
Cu-BVNP	0.013	0.019	0.115	0.116
Mn-BVNP	0.020	0.030	0.095	0.088

**Effects of metal concentration on BVNP absorbance and fluorescence (Stern-Volmer analysis).** The Stern-Volmer method was employed to evaluate the effects of metal concentration on BVNP absorbance and fluorescence behavior. Metal chelation experiments were conducted with higher (100 X, 10 X) and lower (0.1 X and 0.01 X) metal concentrations than for initial experiments. Changes in the absorbance spectra are most apparent for concentrations of 1 X or higher (Fig. S16A). Absorbance at 365 nm and 670 nm both generally decrease with an increase in metal concentration (Fig. S16B-C). The 10 X metal concentration led to the highest fluorescence intensity for 365 nm excitation (Fig. S17A), while the fluorescence intensity in response to 488 nm excitation decreased with increasing metal concentration (Fig. S17B). These results indicate a concentration-dependent effects of metal chelation of BVNP behavior, which is similar to what was observed for BV.

**Comparison of BV and BVNP absorbance and fluorescence behavior.** Since BVNPs are composed of cross-linked biliverdin molecules, we were interested in examining the effects of nanoparticle formation on spectral properties. Direct comparisons of fluorescence intensity or magnitude of absorbance cannot be made between BV and BVNPs since the final concentration of biliverdin in BVNPs is less than the starting concentration because unbound biliverdin was removed from the nanoparticle solution during nanoparticle dialysis. However, observations on the fluorescence emission wavelength, ratio between fluorescence intensity after UV irradiation to fluorescence intensity before UV irradiation, ratio between absorbance after UV irradiation to absorbance before UV irradiation, and qualitative comparisons of absorbance spectra can be made. For 365 nm excitation, BVNPs and Cu-BVNPs exhibit slightly blue-shifted emission peaks compared to their molecular counterparts (Fig. S2, S8). This suggests that biliverdin molecules in BVNPs undergo an aggregation-induced shift in fluorescence emission. Furthermore, the change in fluorescence intensity as a result of UV irradiation was found to be much higher in BV compared to BVNPs (Fig. 1D(ii), Fig. 4E(ii)). This is likely due to a reduction in the conformational

flexibility of biliverdin molecules that have been crosslinked into BVNPs during the nanoparticle synthesis process. Thus, UV irradiation provides a smaller fluorescence advantage for BVNPs than it does for BV because of the conformational changes that UV irradiation induces in BV molecules.

The absorbance ratios before and after UV irradiation, before and after metal chelation in the absence of UV irradiation, and before and after metal chelation in the presence of UV irradiation follow a similar trend for both BV and BVNPs (Fig. S1, Fig. S7). For example, UV irradiation caused minimal change in either BV or BVNP absorbance ratios (Fig. S1 A(i) and B(i), Fig. S7 A(i) and B(i)). Copper-chelated BV and BVNP samples both had a higher absorbance ratio than manganese-chelated BV and BVNP samples. The absorbance spectra shapes for metal-chelated BVNPs also closely match the absorbance spectra shapes of metal-chelated BV (Fig. 1B, Fig. 4C). Like the absorbance spectra of Mn-BV, the absorbance spectra of Mn-BVNP contains multiple Q bands. Like the absorbance spectra of Cu-BV, the Q band for Cu-BVNPs appears blue-shifted compared to that of unchelated samples. These results altogether indicate that the conformational change induced by chelation of each metal was similar between BV and BVNPs. Furthermore, it is apparent that for both BV and BVNPs, UV irradiation is the dominant factor in fluorescence behavior, while metal chelation is the dominant factor in absorbance behavior.

**Potential effects of UV irradiation and metal chelation on conformation of molecules in BVNP.** We also collected circular dichroism (CD) spectra for BVNPs (Fig. S13C). The formation of BVNPs from BV did not lead to a change of peak sign, but led to an overall lower magnitude of the circular dichroism spectra. The effect of UV irradiation is less apparent in the BVNP CD spectra than it is in the BV CD spectra. However, this can be expected from the overall lower effect of UV irradiation on BVNPs compared to its effect on BV.

**Single-particle analysis of BVNP brightness.** Single-particle imaging of BVNPs was conducted with a total internal reflection fluorescence microscopy (TIRFM) system using a 488 nm laser. The average intensity of the particles was found to be higher for Cu-BVNPs than BVNPs or Mn-BVNPs (Fig. S18A). This contrasts with well-plate measurements of the fluorescence emission of BVNPs (Fig. 4F). We then determined the on-time duty cycle (defined as the percentage of each cycle for which the particle is in the “on” state), and examined the product of the on-time duty cycle and the average intensity of the particles (Fig. S18B). Since bulk fluorescence intensity depends on the instantaneous intensity as well as the on-time duty cycle, their product is considered to be a more accurate reflection of bulk-state properties.<sup>46</sup> We found that the product of particle intensity and on-time duty cycle for BVNPs, Cu-BVNPs, and Mn-BVNPs was largely unaffected by the 72 h of UV irradiation, which matches the bulk-state BVNP fluorescence behavior for 488 nm excitation. Similar to bulk-state measurements, BVNP+UV appeared to have a slightly lower product of intensity and on-time duty cycle than BVNP-UV; however, these measurements were within experimental error. These findings further support our hypothesis that the 72 h UV irradiation at 365 nm may “train” the particles for an altered spectral response to only the 365 nm wavelength.

**Single-particle analysis of BVNP photoblinking behavior.** When excited by light, fluorescent nanoparticles cycle between an “on” state in which they are emitting fluorescence, and “off” state in which they are not emitting any fluorescence. This collective

behavior is known as photoblinking. Additionally, when excited by light for long periods of time, nanoparticles can photobleach as other fluorophores do. To evaluate the effects of metal chelation and 72 h UV irradiation of BVNP photoblinking behavior, single-particle analysis was carried out using a TIRFM system as described above. Log-log plots and power law fits of the time on and time off distributions (Fig. 5A) illustrate the effects of metal chelation and 72 h UV irradiation on the time on and time off distributions of the BVNPs. The slopes of the power law fits are provided in Fig. 5B, and the intercept and  $R^2$  values are provided in Figure S19. For BVNP and Mn-BVNP, the magnitude of the time on power law slope decreased as a result of 72 h of UV irradiation, while for Cu-BVNP it slightly increased. The magnitude of the time off power law slope decreased for BVNP and Cu-BVNP as a result of 72 h of UV irradiation, but slightly increased for Mn-BVNP. Additionally, while Cu chelation in the absence of UV irradiation led to a decrease in BVNP time on slope magnitude, it led to an increase in time off slope magnitude. Mn chelation in the absence of UV irradiation led to an increase in magnitude for the time on slope, but had little to no impact on the time off slope. These findings indicate that the effects of metal chelation on time on and time off depends on the chelated metal, and that the time on and time off behavior do not follow the same trend. This suggests that some metals can increase the length of time for which BVNPs are in the “on” state, while others can decrease the time for which BVNPs are in the “on” state. When combined with the lack of a uniform effect from UV irradiation on the time on and time off slopes, this indicates that the BVNP single-particle response to 488 nm cannot be predicted from bulk-state measurements. An alternative illustration of the time on data from Fig. 5A is provided in Fig. S20 in the form of log-log histograms. These histograms reveal the apparent existence of two populations of particles, a majority population that has a low time on, and a much smaller population that has a higher time on. These multiple populations are present regardless of UV irradiation or metal chelation, suggesting that some aspect of BVNP synthesis leads to the formation of particles with multiple subpopulations, each with differing single-particle photoblinking behavior.

Photobleaching time constants (Fig. 5C) were calculated from second-order exponential fits of the time to photobleaching curves (Fig. 5D). Without UV irradiation, copper chelation led to an increase in the first time constant and a decrease in the second time constant, while manganese chelation led to a decrease in both time constants. UV irradiation led to a decrease in the first time constant for BVNPs and Cu-BVNPs, and an increase in time constant for Mn-BVNPs. UV irradiation additionally led to an increase in the second time constant for BVNPs, Cu-BVNPs, and Mn-BVNPs.

We further calculated the single-particle blinking rate (Fig. S21), finding that the particles had a blinking rate of approximately 0.6 to 0.8 Hz. This blinking rate matches closely with our previous reports of carbon dot blinking rates.<sup>46</sup> Regardless of UV irradiation, the blinking rates between BVNPs, Cu-BVNPs, and Mn-BVNPs had overlapping error bars, indicating that 365 nm UV irradiation and metal chelation had little to no effect on the rate of nanoparticle blinking, despite their effects on the nanoparticle time on and time off distributions. Thus, although the length of time for which particles were on or off may have been altered by metal chelation and UV irradiation, the frequency with which the particles would switch between the on and off states remained unaffected.

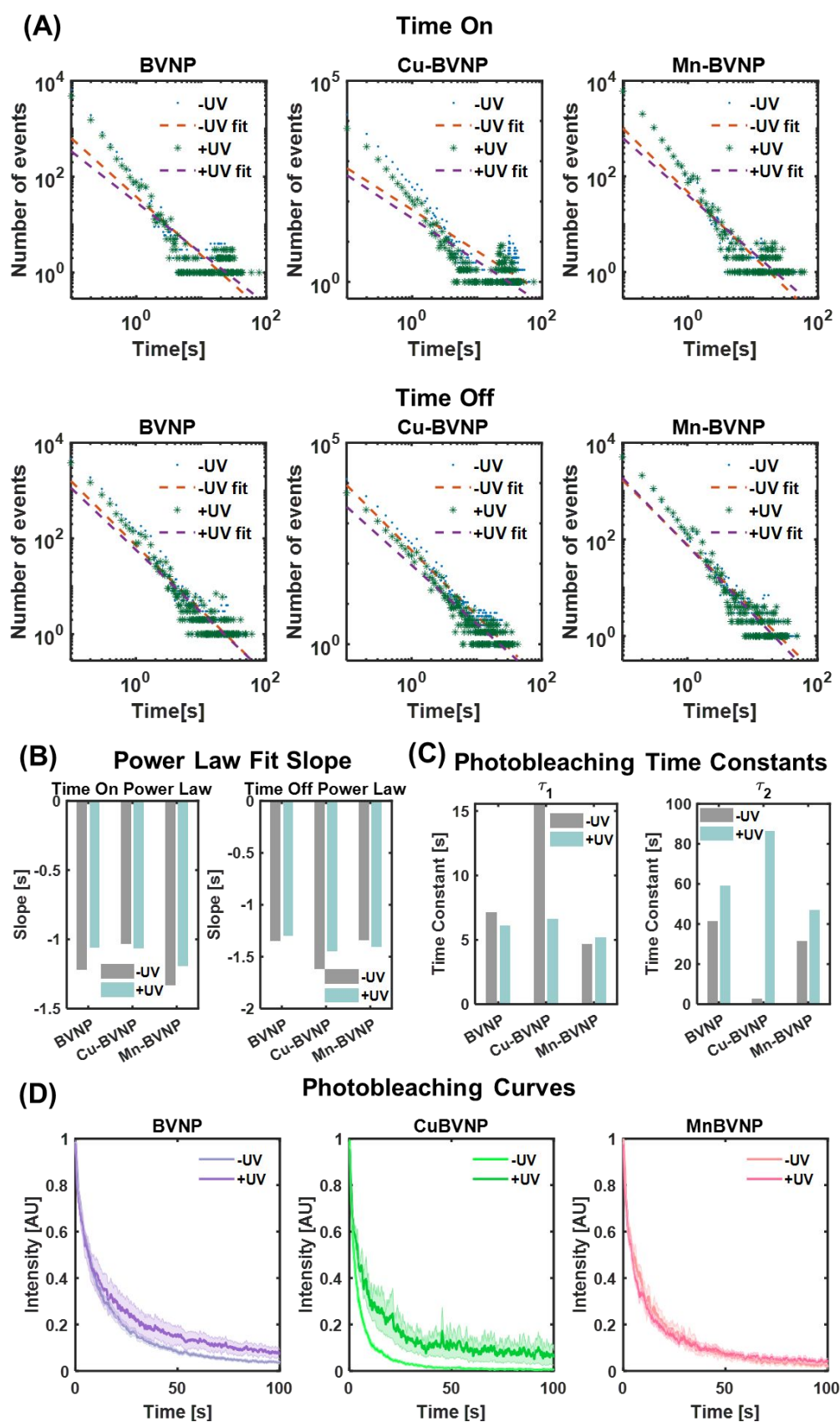
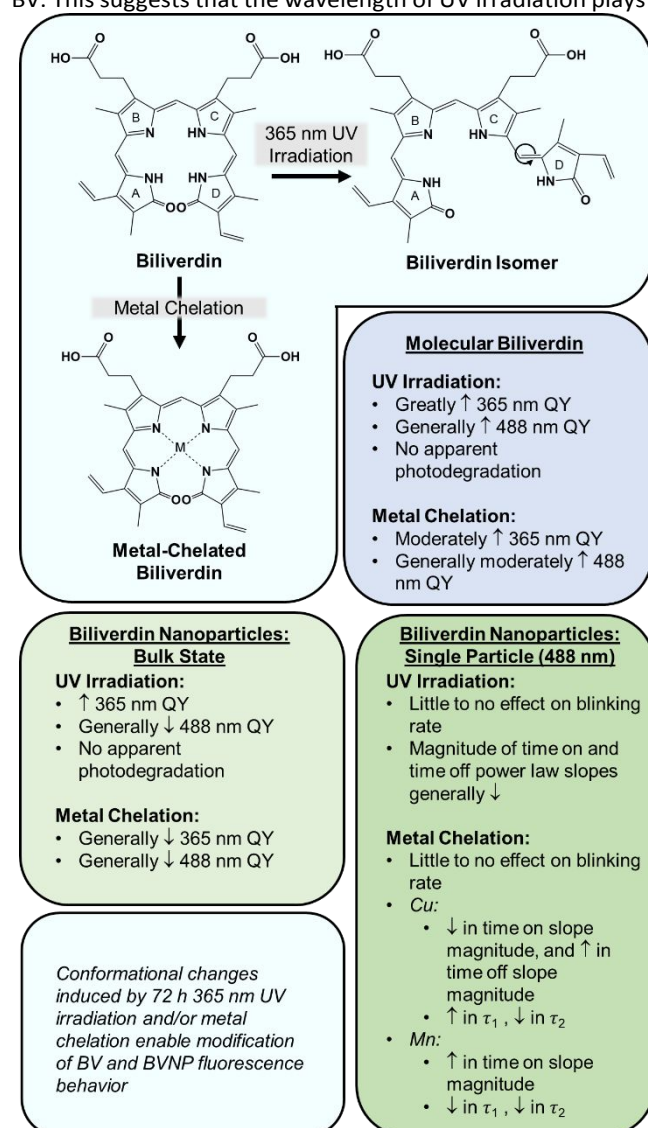


**Figure 5.** Single-particle photoblinking behavior. **(A)** Time on and time off curves and respective power law fits, displaying the number of instances of each on and off time (log-log scale). **(B)** Calculated slopes from time on and time off power law fits. UV irradiation of BVNPs reduces the time on and time off power law slopes. Cu and Mn chelation each have different effects. **(C)** Time constants from single-particle photobleaching experiments. UV irradiation of BVNPs reduces the first time constant and increases the second. Cu and Mn chelation each have different effects on the time constants. **(D)** Photobleaching curves for BVNP, Cu-BVNP, and Mn-BVNP. Envelopes represent standard error of the mean as measured across multiple individual particles.

## Conclusions

The goal of nanomedicine is to develop safer and more effective therapeutic that can be augmented by multiscale imaging.<sup>47-60</sup> In this work, we utilized metal chelation and UV irradiation to alter the spectral properties of biliverdin and biliverdin nanoparticles (**Scheme 2**). We have demonstrated that metal (Co, Cu, Fe, and Mn) chelation and or exposure to 72 h of 365 nm UV irradiation lead to conformational changes in biliverdin. UV irradiation was found to increase BV fluorescence emission for 365 nm excitation without leading to degradation, as confirmed by mass spectrometry. We attribute the change in fluorescence behaviour of UV-irradiated BV to photoisomerization and associated conformational changes. Metal chelation altered the shapes of BV absorbance spectra, and, in the absence of UV irradiation, led to BV fluorescence enhancement for an excitation wavelength of 365 nm. For 488 nm excitation, UV-irradiated metal-chelated BV had little to no change in fluorescence emission compared to metal-chelated BV. This suggests that the wavelength of UV irradiation plays an

important role in modulating the fluorescence emission intensity. Unchelated BV, however, had reduced fluorescence emission for an excitation of 488 nm as a result of 72 h of 365 nm UV irradiation. We further explored the effects of metal (Cu, Mn) chelation and 72 h of 365 nm UV irradiation on biliverdin nanoparticle spectral properties. We found that similar to the effects of these stimuli on BV behavior, BVNPs exhibited altered absorbance and fluorescence spectra. However, the effects of metal chelation and UV irradiation were less drastic for BVNPs than they were in BV. This is likely due to the loss of conformational flexibility in the biliverdin molecules that have been crosslinked to form BVNPs. Using single-particle imaging, we found that the metal used governed the effects of metal chelation on BVNP photobleaching dynamics. Despite this, metal chelation and UV irradiation had no effects on single-particle brightness or photoblinking frequency, suggesting that the relationship between BVNP behavior at the single-particle and bulk-state levels is highly complicated and depends on a number of factors. Overall, this work suggests that conformational changes induced by metal chelation and UV irradiation can be taken advantage of in order to enhance the spectral properties of biliverdin and biliverdin nanoparticles. The dramatic enhancement of fluorescence emission (365 nm excitation) after 72 h of 365 nm UV irradiation suggests that the UV irradiation wavelength may play a role in "training" biliverdin to respond to specific wavelengths. Further studies must be performed to determine whether other irradiation wavelengths also lead to selective enhancement of fluorescence emission for specific excitation wavelengths. Additionally, future experimental work must be conducted to precisely determine the effects of UV irradiation on BV crystal structure. Despite these limitations, the present study provides a detailed exploration of the effects of metal chelation and 365 nm UV irradiation on BV and BVNP behavior, as well as the first demonstration of single-particle imaging of tetrapyrrolic nanoparticles. Furthermore, although biliverdin does not have near-infrared fluorescence emission, the observations made in this work open the potential for similar approaches to be taken to increase the quantum yield of near-infrared-emitting tetrapyrrolic fluorophores and nanoparticles.



**Scheme 2.** Summary of results. UV irradiation leads to photoisomerization of the C15=C16 double bond between the C- and D-rings in biliverdin, leading to conformational changes. Metal chelation also leads to conformational changes, specifically a restriction of biliverdin's conformational flexibility. These stimuli can alter the fluorescence behaviors of biliverdin and biliverdin nanoparticles.

## Conflicts of interest

There are no conflicts to declare.

## Acknowledgements

This project was funded through grants from National Institute of Health, Department of Defense, and University of Illinois. P. Fathi was supported by the National Physical Science Consortium and the National Institute of Standards & Technology through an NPSC graduate fellowship and by the Nadine Barrie Smith Memorial Fellowship from the Beckman Institute. Research reported in this publication was supported by the National Institute of Biomedical Imaging and Bioengineering of the National Institutes of Health under Award Number T32EB019944. This work was carried out in part in the Frederick Seitz Materials Research Laboratory Central Research

Facilities, University of Illinois. We gratefully acknowledge the Chemical and Biomolecular Engineering department shared facilities for access to their fluorescence spectrometer. We also gratefully acknowledge Professor Martin Gruebele and Gopika Gopan for access to and training on the circular dichroism instrument.

### Supporting Information

Supporting information, including materials and methods, quantification of absorbance and fluorescence spectra, Stern-Volmer plots for BV and BVNPs, CD spectra of Co-BV, Cu-BV, Fe-BV, and Mn-BV, FT-IR and CD spectra of BVNPs, and further quantification of single-particle imaging results, is available.

### References

- 1 C. L. Sun, J. Li, X. Z. Wang, R. Shen, S. Liu, J. Q. Jiang, T. Li, Q. W. Song, Q. Liao, H. B. Fu, J. N. Yao and H. L. Zhang, *Chem*, 2019, **5**, 600–616.
- 2 W. Wang, P. Wang, L. Chen, M. Zhao, C. Te Hung, C. Yu, A. A. Al-Khalaf, W. N. Hozzein, F. Zhang, X. Li and D. Zhao, *Chem*, 2020, **6**, 1097–1112.
- 3 D. F. Moyano, Y. Liu, F. Ayaz, S. Hou, P. Puangpoy, B. Duncan, B. A. Osborne and V. M. Rotello, *Chem*, 2016, **1**, 320–327.
- 4 M. Lian, Z. Xue, X. Qiao, C. Liu, S. Zhang, X. Li, C. Huang, Q. Song, W. Yang, X. Chen and T. Wang, *Chem*, 2019, **5**, 2378–2387.
- 5 Z. Dong, L. Feng, Y. Hao, Q. Li, M. Chen, Z. Yang, H. Zhao and Z. Liu, *Chem*, 2020, **6**, 1391–1407.
- 6 X. Han, K. Xu, O. Taratula and K. Farsad, *Nanoscale*, 2019, **11**, 799–819.
- 7 K. Li and B. Liu, *Chem. Soc. Rev.*, 2014, **43**, 6570–6597.
- 8 Y. Jiang and K. Pu, *Small*, 2017, **13**, 1–19.
- 9 R. Garcia-Álvarez, L. Chen, A. Nedilko, A. Sánchez-Iglesias, A. Rix, W. Lederle, V. Pathak, T. Lammers, G. Von Plessen, K. Kostarelos, L. M. Liz-Marzán, A. J. C. Kuehne and D. N. Chigrin, *ACS Photonics*, 2020, **7**, 646–652.
- 10 Y. Park, J. Yoo, M. H. Kang, W. Kwon and J. Joo, *J. Mater. Chem. B*, 2019, **7**, 6271–6292.
- 11 Q. Liu, C. Zhan and D. S. Kohane, *Bioconjug. Chem.*, 2017, **28**, 98–104.
- 12 D. Kim, J. Kim, Y. Il Park, N. Lee and T. Hyeon, *ACS Cent. Sci.*, 2018, **4**, 324–336.
- 13 Y. Liu, P. Bhattarai, Z. Dai and X. Chen, *Chem. Soc. Rev.*, 2019, **48**, 2053–2108.
- 14 S. Eom, G. Choi, H. Nakamura and J. H. Choy, *Bull. Chem. Soc. Jpn.*, 2020, **93**, 1–12.
- 15 Y. Lee, H. Kim, S. Kang, J. Lee, J. Park and S. Jon, *Angew. Chemie - Int. Ed.*, 2016, **55**, 7460–7463.
- 16 Y. Lee, S. Lee, D. Y. Lee, B. Yu, W. Miao and S. Jon, *Angew. Chemie - Int. Ed.*, 2016, **55**, 10676–10680.
- 17 J. Y. Kim, D. Y. Lee, S. Kang, W. Miao, H. Kim, Y. Lee and S. Jon, *Biomaterials*, 2017, **133**, 1–10.
- 18 M. J. Kim, Y. Lee, S. Jon and D. Y. Lee, *Biomaterials*, 2017, **133**, 242–252.
- 19 D. E. Kim, Y. Lee, M. G. Kim, S. Lee, S. Jon and S. H. Lee, *Biomaterials*, 2017, **140**, 37–44.
- 20 D. Y. Lee, J. Y. Kim, Y. Lee, S. Lee, W. Miao, H. S. Kim, J. J. Min and S. Jon, *Angew. Chemie - Int. Ed.*, 2017, **56**, 13684–13688.
- 21 P. Fathi, H. J. Knox, D. Sar, I. Tripathi, S. K. Misra, F. Ostadhosseini, M. B. Esch, J. Chan and D. Pan, *ACS Nano*, 2019, acsnano.9b01201.
- 22 R. Xing, Q. Zou, C. Yuan, L. Zhao, R. Chang and X. Yan, *Adv. Mater.*, 2019, **31**, 1–8.
- 23 P. Fathi and D. Pan, *Nanomedicine*, DOI:10.2217/nmm-2020-0125.
- 24 Q. Yao, R. Chen, V. Ganapathy and L. Kou, *J. Control. Release*, 2020, **328**, 407–424.
- 25 J. W. Singleton and L. Laster, *J. Biol. Chem.*, 1966, **240**, 5518–5525.
- 26 B. Wegiel and L. E. Otterbein, *Front. Pharmacol.*, 2012, **3**, 1–8.
- 27 M. D. Maines, *Physiology*, 2005, **20**, 382–9.
- 28 I. Goncharova and M. Urbanová, *Anal. Biochem.*, 2009, **392**, 28–36.
- 29 G. Wagnière and G. Blauer, *J. Am. Chem. Soc.*, 1976, **98**, 7806–7810.
- 30 M. S. Dimitrijević, J. Bogdanović Pristov, M. Žižić, D. M. Stanković, D. Bajuk-Bogdanović, M. Stanić, S. Spasić, W. Hagen and I. Spasojević, *Dalt. Trans.*, 2019, **48**, 6061–6070.
- 31 J. D. Ostrow and R. V. Branham, *Gastroenterology*, 1970, **58**, 15–25.
- 32 A. Rück, C. Hildebrandt, T. Köllner, H. Schneckenburger and R. Steiner, *J. Photochem. Photobiol. B Biol.*, 1990, **5**, 311–319.
- 33 R. Rotomskis, S. Bagdonas and G. Streckyte, *J. Photochem. Photobiol. B Biol.*, 1996, **33**, 61–67.
- 34 L. Pan, X. Wang, S. Yang, X. Wu, I. Lee, X. Zhang, R. A. Rupp and J. Xu, *PLoS One*, 2012, **7**, 1–6.
- 35 M. Uttamlal and A. Sheila Holmes-Smith, *Chem. Phys. Lett.*, 2008, **454**, 223–228.
- 36 M. Dayer, A. Moosavi-Movahedi and M. Dayer, *Protein Pept. Lett.*, 2010, **17**, 473–479.
- 37 E. Consiglieri, A. Gutt, W. Gärtner, L. Schubert, C. Viappiani, S. Abbruzzetti and A. Losi, *Photochem. Photobiol. Sci.*, 2019, **18**, 2484–2496.
- 38 K. C. Toh, E. A. Stojković, I. H. M. Van Stokkum, K. Moffat and J. T. M. Kennis, *Proc. Natl. Acad. Sci. U. S. A.*, 2010, **107**, 9170–9175.
- 39 A. Björling, O. Berntsson, H. Lehtivuori, H. Takala, A. J. Hughes, M. Panman, M. Hoernke, S. Niebling, L. Henry, R. Henning, I. Kosheleva, V. Chukharev, N. V. Tkachenko, A. Menzel, G. Newby, D. Khakhulin, M. Wulff, J. A. Ihalainen and S. Westenhoff, *Sci. Adv.*, DOI:10.1126/sciadv.1600920.
- 40 C. Wang, M. L. Flanagan, R. D. McGillicuddy, H. Zheng, A. R. Ginzburg, X. Yang, K. Moffat and G. S. Engel, *Biophys. J.*, 2016, **111**, 2125–2134.
- 41 D. J. Heyes, S. J. O. Hardman, M. N. Pedersen, J. Woodhouse, E. De La Mora, M. Wulff, M. Weik, M. Cammarata, N. S. Scrutton and G. Schirò, *Commun. Biol.*, 2019, **2**, 1–8.
- 42 A. A. Samma, C. K. Johnson, S. Song, S. Alvarez and M. Zimmer, *J. Phys. Chem. B*, 2010, **114**, 15362–15369.
- 43 M. O. Senge, S. A. MacGowan and J. M. O'Brien, *Chem. Commun.*, 2015, **51**, 17031–17063.
- 44 C. H. Chiang, D. Pangeni and E. E. Nesterov, *Macromolecules*, 2017, **50**, 6961–6966.
- 45 D. Pangeni and E. E. Nesterov, *Macromolecules*, 2013, **46**,

- 7266–7273.
- 46 P. Fathi, J. S. Khamo, X. Huang, I. Srivastava, M. B. Esch, K. Zhang and D. Pan, *Carbon N. Y.*, 2019, **145**, 572–585.
- 47 S. K. Datta, S. K. Misra, M. L. Saha, N. Lahiri, J. Louie, D. Pan, P. J. Stang, *Proceedings of the National Academy of Sciences* 2018, **115** (32), 8087-8092
- 48 M. S. Khan, S. K. Misra, K. Dighe, Z. Wang, A. S. Schwartz-Duval, D. Sar, D. Pan, *Biosensors and Bioelectronics* 2018, **110**, 132-140
- 49 M. S. Khan, K. Dighe, Z. Wang, I. Srivastava, E. Daza, A. S. Schwartz-Dual, J. Ghannam, S. K. Misra, D. Pan, 2018 *Analyst* **143** (5), 1094-1103
- 50 I. Srivastava, S. K. Misra, F. Ostadhossein, E. Daza, J. Singh and D. Pan, *Nano Research* 2017, **10** (10), 3269-3284
- 51 S. K. Misra F. Ostadhossein, R. Babu, J. Kus, D. Tankasala, A. Sutrisno, K. A. Walsh, C. R. Bromfield, D Pan, *Advanced Healthcare Materials* 2017, **6** (11), 1700008
- 52 F. Ostadhossein and D. Pan, *Wiley Interdisciplinary Reviews: Nanomedicine and Nanobiotechnology* 2016, **9** (3), e1436
- 53 S. K. Misra, I. Srivastava, I. Tripathi, E. Daza, F. Ostadhossein, D. Pan, *Journal of the American Chemical Society* 2017, **139** (5), 1746-1749
- 54 M. S. Khan, S. K. Misra, Z. Wang, E. Daza, A. S. Schwartz-Duval, J. M. Kus, D. Pan, and D. Pan, *Analytical chemistry* 2017, **89** (3), 2107-2115
- 55 S. K. Misra, F. Ostadhossein, E. Daza, E. V. Johnson, D. Pan, *Advanced Functional Materials* 2016, **26** (44), 8031-8041
- 56 S. K. Misra, G. Ghoshal, M. R. Gartia, Z. Wu,] A. K. De, M. Ye, C. R. Bromfield, E. M. Williams, K. Singh, K. V. Tangella, L. Rund, K. Schulten, L. B. Schook, P. S. Ray, E. C. Burdette, and D. Pan, *ACS Nano* 2015, **9** (11), 10695-10718
- 57 S. K. Misra, H. H. Chang, P. Mukherjee, S. Tiwari, A. Ohoka, D. Pan, *Scientific reports* 2015, **5**, 14986
- 58 P. Mukherjee, S. K. Misra, M. C. Gryka, H. H. Chang, S. Tiwari, W. L. Wilson, *Small* 2014, **11** (36), 4691-4703
- 59 D. Soodgupta, D. Pan, G. Cui, A. Senpan, X. Yang, L. Lu, K. N. Weilbaecher, E. V. Prochownik, G. M. Lanza, M. H. Tomasson, *Molecular Cancer Therapeutics* 2015, **14** (6), 1286-1294
- 60 S. K. Misra, T. W. Jensen, D. Pan. *Nanoscale* 2015, **7** (16), 7127-7132